Simulations of a simplified LOCA scenario with a non-equilibrium homogeneous model

Olivier Hurisse, Lucie Quibel

Simulations of a simplified LOCA scenario with a non-equilibrium homogeneous model.

Olivier Hurisse[1], Lucie Quibel[1,2]

1 - EDF Lab Chatou, 6 quai Watier, 78400 Chatou, FRANCE.
2 - IRMA, UMR CNRS 7501, 7 rue Descartes, 67000 Strasbourg, FRANCE.

Abstract

The LOCA scenario involves strong and sudden depressurization of hot liquid water, which generates strong pressure waves propagating through the primary circuit devices. Due to these severe conditions, the induced vaporization of the liquid water occurs under thermodynamical conditions that may be far from the thermodynamical equilibrium. The accurate numerical prediction of this kind of accidental scenarii, and of their potential consequences, then requires numerical tools that are able to deal with non-equilibrium two-phase thermodynamics. A specific module is being developed by EDF Lab Chatou in the framework of *Code_Saturne* in order to assess such severe accidental situations involving liquid-vapor flows. The aim of this paper is to present the model and the numerical schemes that have been developed. Some numerical results are also compared to the experimental measurements obtained thanks to the SUPERCANON facility, which allowed to reproduce the first stage of a LOCA scenario.

KEYWORDS

LOCA, non-equilibrium thermodynamics, two-phase flows, mass transfer

1 Introduction

Some accidental scenarii studied in the framework of the nuclear safety analysis involve liquids undergoing strong pressure drops at high temperature (as the LOCA scenario for instance). In order to perform realistic simulations of such situations, a code based on a model that can handle both the thermodynamical disequilibrium between liquid and vapor and complex equations of state is required.

We present here a code based on a homogeneous model which allows to handle non-equilibrium two-phase flows [1, 2, 3, 4]. The latter is built on the

basis of the Euler system of equations and complemented by a mixture pressure law. This mixture pressure is defined in accordance with the Gibbs relation on the basis of the phasic pressures which are defined through a look-up table [4] based on the IAPWS-97 formulation [5].

The overall numerical scheme relies on a fractional step approach [6] and uses a Lie-Trotter spliting. It thus treats separately the convection terms and the source terms, which account for the return to the thermodynamical equilibrium. Due to the complex equation of state furnished by the look-up tables described in section 3, a relaxation scheme [7] has been chosen for the computation of the numerical convective fluxes. In [4], it appears to be a very good compromise between accuracy and stability. Thanks to the linearity of the source terms, their discretization can be performed through a simple Euler implicit scheme.

At last, a simple test case of vaporization of hot pressurized liquid is proposed. This test case is based on the results of the SUPERCANON facility[8] which has been designed in order to be representative of a LOCA in the primary circuit of a PWR nuclear reactor.

2 The homogeneous non-equilibrium model

In this section, the considered model is only briefly presented. The whole building approach is available for instance in [1, 2, 3, 4]. Thermodynamically, each phase $k = l, v$ (liquid or vapor) is described by its own complete equation of state, expressed as a specific entropy $s_k(\tau_k, e_k)$ $(JK^{-1}kg^{-1})$ as a function of τ_k the specific volume (m^3kg^{-1}) and e_k the specific energy (Jkg^{-1}) and satisfying the Gibbs relation:

$$T_k ds_k = de_k + P_k d\tau_k, \tag{1}$$

where the thermodynamical pressure P_k and the temperature T_k are then defined as derivatives of the specific entropy:

$$\frac{1}{T_k} = \left.\frac{\partial s_k}{\partial e_k}\right|_{\tau_k} \quad ; \quad \frac{P_k}{T_k} = \left.\frac{\partial s_k}{\partial \tau_k}\right|_{e_k}. \tag{2}$$

Let us introduce the volume fraction α_k, the mass fraction y_k and the energy fraction z_k of phase k:

$$Y_k = (\alpha_k, y_k, z_k). \tag{3}$$

These fractions satisfy the following conservation relations:

$$1 = \alpha_l + \alpha_v \quad ; \quad 1 = y_l + y_v \quad ; \quad 1 = z_l + z_v, \tag{4}$$

and vary in accordance with the second principle of thermodynamics. Thanks to these fractions, phasic quantities can be expressed from the mixture specific volume τ and from the mixture specific energy e:

$$\tau_k = \frac{\alpha_k}{y_k}\tau \quad ; \quad e_k = \frac{z_k}{y_k}e. \tag{5}$$

Moreover, thanks to the constraints (4) which states that $Y_l + Y_v = (1,1,1)$, the model will be defined on the sole basis of the liquid fractions (or vapor fractions). We thus set here $Y = Y_l$ for convenience. The mixture entropy s is then defined as a function of Y, e, and τ:

$$s(Y,\tau,e) = y_l s_l(\tau_l, e_l) + y_v s_v(\tau_v, e_v). \tag{6}$$

A Gibbs relation can be written for the mixture entropy s by deriving (6):

$$ds = \frac{\partial s}{\partial e}_{|Y,\tau} de + \frac{\partial s}{\partial \tau}_{|Y,e} d\tau + \nabla_{Y|e,\tau}(s) \cdot dY.$$

By identifying the different terms, this allows to define a temperature law and a pressure law for the mixture:

$$\frac{P}{T}(Y,\tau,e) = \frac{\partial s}{\partial \tau}_{|Y,e} \quad ; \quad \frac{1}{T}(Y,\tau,e) = \frac{\partial s}{\partial e}_{|Y,\tau}. \tag{7}$$

Then, using the definitions (2) and (5), the thermodynamical mixture quantities can be written on the basis of the phasic ones:

$$P(Y,\tau,e) = \frac{\alpha_l \frac{P_l}{T_l} + \alpha_v \frac{P_v}{T_v}}{\frac{z_l}{T_l} + \frac{z_v}{T_v}} \quad ; \quad \frac{1}{T}(Y,\tau,e) = \frac{z_l}{T_l} + \frac{z_v}{T_v}. \tag{8}$$

Thanks to the definition of these quantities, the thermodynamical behavior of the two-phase mixture is completely defined. In order to account for the dynamical aspect of the flows, the velocity equilibrium is assumed. The following set of partial differential equations can thus be proposed on the basis of the classical Euler set of equations:

$$\begin{cases} \dfrac{\partial}{\partial t}(\rho Y) + \dfrac{\partial}{\partial x}(\rho U Y) = \rho \Gamma, \\ \dfrac{\partial}{\partial t}(\rho) + \dfrac{\partial}{\partial x}(\rho U) = 0, \\ \dfrac{\partial}{\partial t}(\rho U) + \dfrac{\partial}{\partial x}\left(\rho U^2 + P\right) = 0, \\ \dfrac{\partial}{\partial t}(\rho E) + \dfrac{\partial}{\partial x}(U(\rho E + P)) = 0. \end{cases} \tag{9}$$

We recall that Y is a vector of $[0,1]^3$ and hence the source term Γ is a vector of $\mathbb{R}^3$. It reads:

$$\Gamma = \left(\frac{\bar{\alpha}_l - \alpha_l}{\lambda}, \frac{\bar{y}_l - y_l}{\lambda}, \frac{\bar{z}_l - z_l}{\lambda} \right),$$

where $(\bar{\alpha}_l, \bar{y}_l, \bar{z}_l)$ are the equilibrium fractions which maximize the mixture entropy for a given (τ, e). In system (9), U stands for the velocity of the mixture (velocity are assumed to be equal for the two phases), ρ for its density, and E denotes the total specific energy: $E = e + U^2/2$. It can be proved that this choice

of source terms agrees with the second law of thermodynamics (see [1, 2, 3, 4] among others). The time scale $\lambda > 0$ rules the return to the thermodynamical equilibrium. In other words, when $\lambda \to 0$, the two phases are assumed to be at thermodynamical equilibrium, which means that the phasic pressures, the phasic temperature and the phasic Gibbs enthalpies are equal.

In this model, the user must specify one EOS for the specific entropies s_k (one for each phase) and the time-scale $\lambda > 0$ which can depend on the thermodynamical quantities.

3 Specification of the EOS by a look-up table

When dealing with water thermodynamics, it is important to specify accurate EOS for the entropies s_k. Unfortunately, the classical analytical EOS are often not accurate enough in order to deal with situations where the thermodynamical range of pressure and temperature are important, as in the LOCA scenario. The IAPWS formulation [5] has thus been considered here and, to save computational time, a look-up table (named LuT in the following) has been implemented [4]. We describe here how this LuT is built. Since the model deals with non-equilibrium thermodynamics and since each phase has to possess its own EOS, a LuT is built for each phase.

The (P, T)-plane is chosen as an entry of the LuT and the Gibbs free enthalpy $\mu_k(P, T)$ is given for each phase [9]. In order to remain consistent with the Gibbs relation for each phase (1), all the other quantities have to be computed from the derivatives of

$$\mu_k(P, T) = e_k(P, T) + P\tau_k(P, T) - Ts_k(P, T).$$

Indeed, by differentiating μ_k and by using the phasic Gibbs relation (1) we get:

$$d\mu_k = \tau_k dP - s_k dT,$$

so that the specific volume and the specific entropy are respectively defined as:

$$\tau_k(P, T) = \partial\mu_k/\partial P_{|T} \quad \text{and} \quad s_k(P, T) = -\partial\mu_k/\partial T_{|P}.$$

The specific energy then follows $e_k(P, T) = \mu_k(P, T) - P\tau_k(P, T) + Ts_k(P, T)$.

Remark. *In order to fulfill the phasic Gibbs relation (1), the quantities τ_k, s_k and e_k should not be tabulated independently.*

As in [10], the thermodynamical plane (P, T) is discretized using a Quadtree approach which is balanced to get a regular discretization of the plane, enabling a quick research through the look-up table in practical simulations. Some domains of the (P, T)-plane are refined. This is actually the case: in the neighborhood of the saturation curve, at low pressures, at low temperatures and at high pressures on the saturation curve. The LuT used in the next sections has been built for pressures from 0.1 bar to 219 bars, so that we avoid vicinity of the critical point. The temperature range is $[283.0\ K; 1070.0\ K]$.

Figure 1 shows some visualizations of the quadtree mesh for different ranges of pressures and temperatures. On each cell of the (P,T)-plane, the IAPWS-97 Gibbs enthalpy μ_k is interpolated using a polynomial spline in P and T. The most important point is to preserve the Gibbs relations (1). It is required that μ_k belongs to $\mathcal{C}^1$ on the whole domain. Therefore, cubic splines are used and a specific treatment is applied to each cell connected to wider cells. For these cells, at each node that is common with a wider cell, the values of μ_k and its derivatives are not obtained from IAPWS-97. These values are replaced by the values of μ_k and its derivatives computed from the interpolated spline of the wider cell. Hence we ensure the continuity of the interpolated value μ_k and of its derivatives with respect to P and T at the junction between the cells of different sizes. For this purpose, the computation of the spline coefficients is then done by decreasing order of the size of the cells. The final level of refinement of the quadtree is chosen so as to get a relative error between the IAPWS values of μ_k and the interpolated values less than a threshold. In the LuT used in the next sections, this threshold has been chosen equal to 10^{-5}, and the final mesh contains more than 163000 cells.

The use of meshes based on quadtree techniques is a great advantage because it allows the local refinement of the description together with a reasonable computational cost for the search of the cell in which the properties have to be estimated. In fact, for a given (P^0,T^0), the cost of the search of the quadtree's cell containing (P^0,T^0) is proportional to the depth of this cell in the quadtree structure (i.e. the smaller the target cell is, the more expensive its search is).

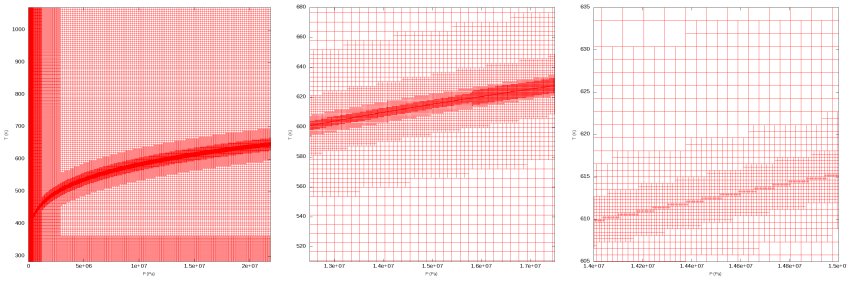

Figure 1: Mesh of the (P,T)-plane. The left figure shows the whole mesh, and the log-like domain corresponds to the mesh refinement around the saturation curve. The two figures on the right show zooms on the saturation curve zone.

We are dealing with compressible phenomena so that the model of section 2 has to be discretized in conservative form (numerical schemes are described in section 4). Hence the "natural" variables for the conservative part of the model are (τ,e). Since the LuT EOS is defined in the (P,T)-plane, and in order to maintain the consistency of the thermodynamical description through a complete LuT, we need to compute the change of variables $(\tau_k,e_k)\mapsto(P_k,T_k)$. More precisely, for any value of the specific volume τ_k^0 and specific energy e_k^0,

we have to find the pressure P_k and the temperature T_k that fulfill:

$$\begin{cases} e_k(P_k, T_k) = e_k^0, \\ \tau_k(P_k, T_k) = \tau_k^0, \end{cases} \tag{10}$$

where the functions $(P_k, T_k) \mapsto e_k(P_k, T_k)$ and $(P_k, T_k) \mapsto \tau_k(P_k, T_k)$ are obtained from the LuT. From a numerical point of view, the computation of an approximate solution of (10) through a Newton-type algorithm can be tricky and it requires an accurate initial guess of the solution. For this purpose, a second LuT has been built for each phase. This second LuT is based on a non-balanced quadtree for the (τ, e)-plane. At each vertice (τ_k^i, e_k^i) of the mesh corresponds a couple (P_k^i, T_k^i) such that $e_k(P_k^i, T_k^i) = e_k^i$ and $\tau_k(P_k^i, T_k^i) = \tau_k^i$. This second LuT is not used directly, but using bilinear interpolation, it represents a database to provide initial guesses to solve the general problem (10). With the help of this second LuT, solving (10) requires less iterations and it is more robust. For the sections below, this second LuT contains 166000 cells.

Remark. *In practice, considering the Stiffened Gas EOS as a reference, the order of magnitude of the computation costs is 700 times higher for the direct IAPWS formulation and it is 8 times higher with the LuT EOS as depicted above. Obviously, the gain in CPU time strongly depends on the test case and on the LuT used (the local refinement and the depth of the quadtree are strongly involved).*

4 Numerical schemes

The overall numerical method is based on a fractional step method [6] using a Lie-Trotter splitting. The initial condition problem associated with system of equations (9) can be written:

$$\frac{\partial}{\partial t}(W) = -\frac{\partial}{\partial x}(\mathcal{F}(W)) + \mathcal{G}(W), \quad W(t=0) = W^0, \tag{11}$$

where $\mathcal{F}$ correspond to the convective flux and $\mathcal{G}$ to the source terms. A straightforward Lie-Trotter splitting has been chosen here. It consists in solving at time $t = t^n$ the following two sub-systems during a time step Δt^n:

$$(i) \quad \frac{\partial}{\partial t}(W_a) = -\frac{\partial}{\partial x}(\mathcal{F}(W_a)), \quad W_a(t^n) = W^n, \tag{12}$$

which gives $W_a(t^n + \Delta t^n)$;

$$(ii) \quad \frac{\partial}{\partial t}(W_b) = \mathcal{G}(W_b), \quad W_b(t = t^n) = W_a(t^n + \Delta t^n). \tag{13}$$

Since this splitting is first order with respect to time, each sub-system is solved using first order schemes.

The first sub-system takes into account the convective part. For that purpose, first-order explicit and conservative finite volumes schemes are used. Their

general form for a one-dimensional framework with cells Ω_i is:

$$|\Omega_i|(W_i^{n+1} - W_i^n) = -\Delta t^n((F(W_i^n, W_{i+1}^n) - F(W_{i-1}^n, W_i^n)), \qquad (14)$$

where W_i^n denotes the space-average value of W on the cell Ω_i at time t^n. The time step Δt^n is computed from the variable W_i^n and from the mesh size $|\Omega_i|$ in order to fulfill stability constraint. The two-point numerical flux F depends on the used scheme. In the following, the results obtained with the relaxation scheme [7] are presented.

The second sub-system (13) corresponds to a system of ordinary derivative equations. In this sub-system, the return to equilibrium is accounted for. Since the time-step is computed to fulfill a stability constraint of the numerical scheme used for the first sub-system, this second step is achieved using an Euler implicit scheme. The latter becomes very easy to solve thanks to the linear source terms Γ involved in the model.

The numerical schemes have been submitted to several verification test cases based on Riemann problems (see [4]).

5 Comparisons with some SUPERCANON results

The present test case is associated to the experimental facility SUPERCANON [8]. It was set up to measure the sudden depressurization of heated water from 150 $bars$ to 1 bar, which is representative of a LOCA in the primary circuit of a PWR. Figure 2 is a sketch of the facility. A tube (100 mm of inner diameter and 4.389 m long) is filled with water and closed with a cap. The water is heated and when the operating conditions are reached (in pressure and temperature), the cap is released by a system based on an exploding cordon and is supposed to be almost instantaneous with respect to the fluid phenomena. The pressure in the tube is measured at six different locations $P_{1,..,6}$, and the vapor fraction is measured at the point P_t (see figure 2). Three different initial temperatures have been tested for the liquid water in the tube: $280°C$, $300°C$ and $320°C$, which respectively correspond to: the temperature at the inlet of the core, the mean temperature in the core and the temperature at the outlet of the core. Moreover, different breach diameters have been used at the outlet of the tube, but we only focus here on the case with a fully opened tube. We also restrict ourselves to the initial temperature of $300°C$.

The scenario of the experiment is the following [11]. When the cap is released, a "saturation" wave travels from the cap location to the end of the tube. Due to this wave, the temperature in the pipe remains almost constant and the pressure drops to the saturation pressure at the initial temperature: $P = P_{sat}(573.15\ K) = 86\ 10^5\ Pa$. Then, a vaporisation front travels into the pipe and the vapor fraction starts to increase. The vaporisation front is a two-phase phenomenon and it travels much slower than the "saturation" wave

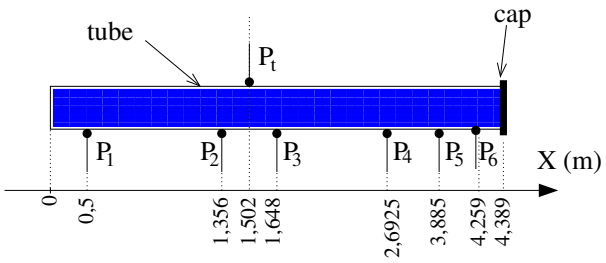

Figure 2: Sketch of the SUPERCANON configuration. The pressure is measured at the points $P_1, ..., P_6$ and the vapor fraction is measured at the point P_t.

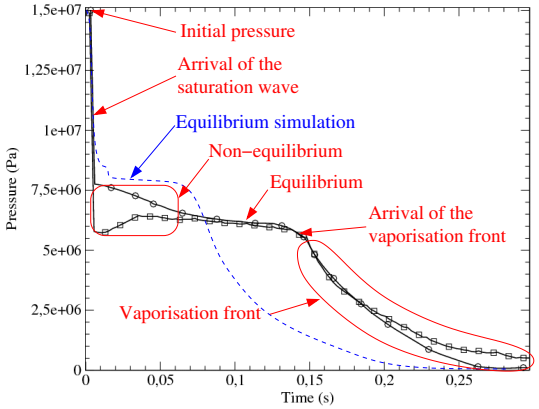

Figure 3: Sketch of the time evolution of the pressure at the points P_1. The black curves represent experimental measurements for two different runs (for the same conditions). The blue curve represents the pressure profile simulated when considering the thermodynamical equilibrium.

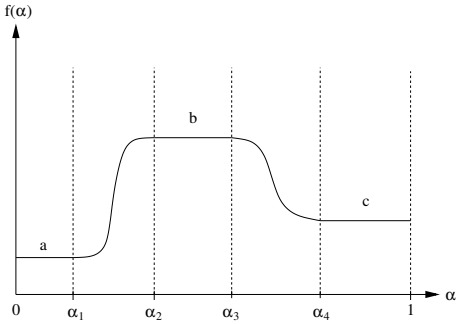

Figure 4: Definition of the function $\alpha \in [0,1] \mapsto f(\alpha)$ used for the definition of λ.

which occurs in pure liquid water. Through the vaporisation front, the vapor fraction increases and both the pressure and the temperature drop again. The sketch of the time evolution of the pressure at points P_1 is plotted on figure 3 for two different experimental runs based on the "same conditions". The blue curve represents the pressure profile at P_1 when enforcing the thermodynamical equilibrium in the simulations. For this experimental setting, the numerical results obtained by considering the thermodynamical equilibrium seems not in agreement with the experimental data?

Indeed, for this experiment, the two phases are likely to be out of the thermodynamical equilibrium [12]. As a consequence, the response of the model should be sensitive to the choice of the time-scale λ. It is not easy to derive a general law for λ on the basis of physical considerations, even if some attempts have been done on the basis of the nucleation theory [4]. For this reason, we propose here a law built following the observations reported in [13], on the basis of an experiment of a flashing (steady) flow in a divergent duct. This law combines two terms: one term that diminishes the relaxation time-scale when the flow is too far from equilibrium ; and one term that decreases the relaxation time-scale when the steam fraction increases. This law is not built on mechanical assumptions and it must be seen as a "toy law" whose parameters have been chosen to fit the experiments. We follow here the same kind of form than the one proposed in [14]:

$$\lambda = \lambda_0 \ f(\alpha_v) \ e^{-\left(\frac{|\alpha_v - \overline{\alpha}_v|}{\delta\alpha}\right)^2},$$

where the function $\alpha \in [0,1] \mapsto f(\alpha)$ corresponds to 3 constant values with cosine connections to get a smooth function, as defined on figure 4. The law used to compute the results presented below has the following parameters : $\lambda_0 = 10^{-2}$ s et $\delta\alpha = 2.9\ 10^{-3}$, $a = 1$, $b = 0.05$, $c = 0$, $\alpha_1 = 0$, $\alpha_2 = 0.15$, $\alpha_3 = 0.25$, $\alpha_4 = 0.65$.

The numerical results have been obtained on a one-dimensional domain with a length of 10 m. The domain $0 < x < 4.389$ m is filled with pure water at 150 $bars$ and $300°C$. Actually, the numerical model can not handle incondensable gases. Hence the domain $4.389\ m < x < 10\ m$, which should be filled with air at 1 bar and $20°C$, is filled with hot steam at 1 bar and $300°C$. The left boundary condition at $x = 0$ is a wall and the right boundary condition at $x = 10$ m is an outlet. Figures 5 show the pressure computed by the code at point P_1 with respect to time. Numerical approximations have been computed for several meshes containing respectively 300, 1000, 3000 and 9000 uniform cells on the whole domain. The parameters of the law for λ have been chosen in order to fit the experiment for the finest mesh. One can nevertheless observe a very good agreement between experiment and numerical simulations for all the meshes. Moreover, it can be noticed that the difference between the numerical results for 3000 and 9000 cells is small, which means that the results seem almost converged for these finest meshes.

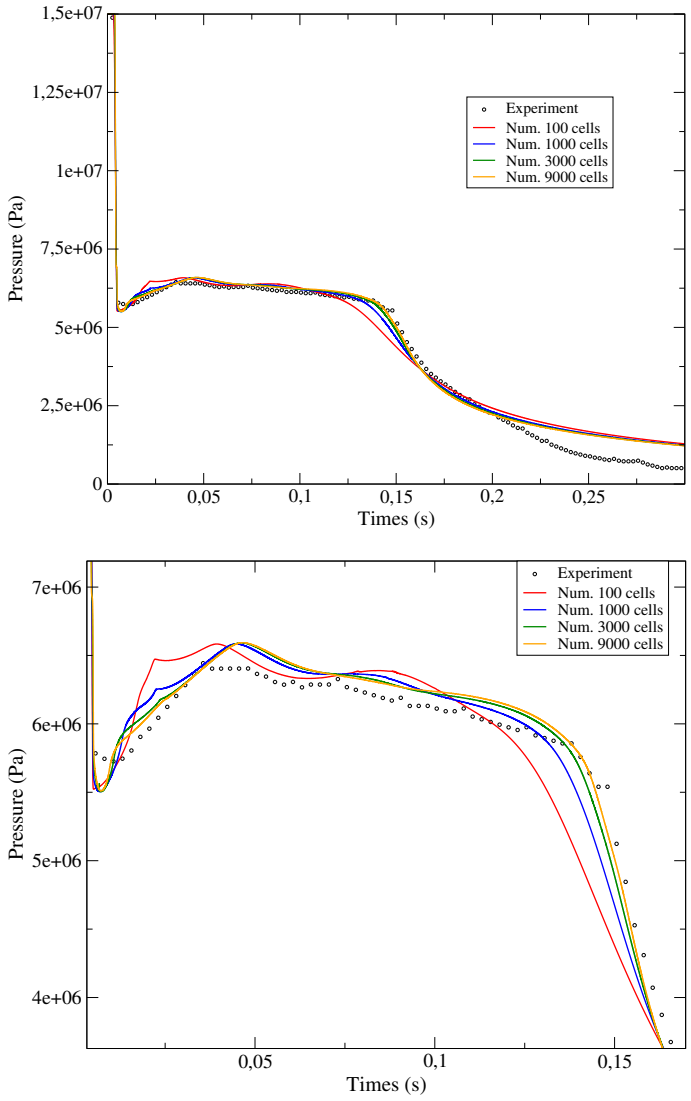

Figure 5: Comparison between the experiment and the numerical results for the pressure at point P_1. The figure on the bottom corresponds to a zoom around the "saturation plate".

6 Conclusion

The model described in section 2 seems very promising when coupled to a complex and accurate EOS as the one presented in section 3. The comparison of section 5 suggests that with an appropriate choice of the time scale λ, which rules the return to the thermodynamical equilibrium, a very good agreement could be obtained with experimental results of sudden depressurization of hot liquid water. Obviously, the law proposed in section 5 is a toy law and it is not satisfactory if one aims at building a predictive numerical tool. Some work has thus been initiated in [4] in order to propose time scale laws based on the classical nucleation theory.

Acknowledgments

The second author receives a financial support by ANRT through an EDF/CIFRE grant number 2017/0476. Computational and neuronal facilities were provided by EDF.

References

[1] T. Barberon and P. Helluy, "Finite volume simulation of cavitating flows," *Computers and Fluids*, **34** (7), pp. 832–858 (2005).

[2] J. Jung, *Numerical simulations of two-fluid flow on multicores accelerator*, PhD thesis, Université de Strasbourg, 2013, https://tel.archives-ouvertes.fr/tel-00876159.

[3] O. Hurisse and L. Quibel, "A homogeneous model for compressible three-phase flows involving heat and mass transfer.," *ESAIM: Proceedings and Surveys*, **66**, pp. 81–108 (2019).

[4] P. Helluy, O. Hurisse, and L. Quibel, "Assessment of numerical schemes for complex two-phase flows with real equations of state.," *Computers & Fluids* (2019).

[5] W. Wagner and H.-J. Kretzschmar, *International Steam Tables: Properties of Water and Steam Based on the Industrial Formulation IAPWS-IF97*, Springer-Verlag Berlin Heidelberg (2008).

[6] N. Yanenko, *Méthode à pas fractionnaires: résolutions de problèmes polydimensionnels de physique mathématique*, Collection Intersciences, A. Colin (1968).

[7] C. Chalons and J.-F. Coulombel, "Relaxation approximation of the Euler equations," *Journal of Mathematical Analysis and Applications*, **348** (2), pp. 872 – 893 (2008).

[8] B. Riegel, *Contribution à l'étude de la décompression d'une capacité en régime diphasique*, PhD thesis, Université de Grenoble, 1978.

[9] G. Faccanoni and H. Mathis, "Admissible Equations of State for Immiscible and Miscible Mixtures," *ESAIM: Proceedings and Surveys*, **66**, pp. 1–21 (2019).

[10] M. Hoffmann, *An Explicit Discontinuous Galerkin Method for Parallel Compressible Two-Phase Flow*, PhD thesis, University of Stuttgart, 2017.

[11] A. Edwards and T. O'Brien, "Studies of phenomena connected with the depressurization of water reactors," *Journal of the British Nuclear Energy Society*, **9**, pp. 125–135 (1970).

[12] J. Bartak, "A study of the rapid depressurization of hot water and the dynamics of vapour bubble generation in superheated water," *International Journal of Multiphase Flow*, **16** (5), pp. 789–798 (1990).

[13] Z. Bilicki, R. Kwidziński, and S. A. Mohammadein, "Evaluation of the relaxation time of heat and mass exchange in the liquid-vapour bubble flow," *International journal of heat and mass transfer*, **39** (4), pp. 753–759 (1996).

[14] O. Hurisse, "Numerical simulations of steady and unsteady two-phase flows using a homogeneous model," *Computers and Fluids*, **152**, pp. 88–103 (2017).